PLOS ONE

RESEARCH ARTICLE

Hybrid nanocomposite curcumin-capped gold nanoparticle-reduced graphene oxide: Anti-oxidant potency and selective cancer cytotoxicity

Lina A. Al-Ani[1☯], Wageeh A. Yehye[1☯*], Farkaad A. Kadir[2☯], Najihah M. Hashim[3,4‡], Mohammed A. AlSaadi[1,5,6☯], Nurhidayatullaili M. Julkapli[1☯*], Vincent K. S. Hsiao[7‡]

1 Institute of Postgraduate Studies, Nanotechnology & Catalysis Research Centre (NANOCAT), University of Malaya, Kuala Lumpur, Malaysia, **2** Department of Anatomy and Medical Imaging, Faculty of Medical and Health Sciences, University of Auckland, Auckland, New Zealand, **3** Department of Pharmacy, Faculty of Medicine, University of Malaya, Kuala Lumpur, Malaysia, **4** Centre for Natural Products and Drug Discovery (CENAR), University of Malaya, Kuala Lumpur, Malaysia, **5** University of Malaya Centre for Ionic Liquids (UMCiL), University of Malaya, Kuala Lumpur, Malaysia, **6** National Chair of Materials Sciences and Metallurgy, University of Nizwa, Nizwa, Sultanate of Oman, **7** Department of Applied Materials and Optoelectronic Engineering, National Chi Nan University, Nantou, Taiwan

☯ These authors contributed equally to this work.
‡ These authors also contributed equally to this work.
* wdabdoub@um.edu.my (WAY); nurhidayatullaili@um.edu.my (NMJ)

Citation: Al-Ani LA, Yehye WA, Kadir FA, Hashim NM, AlSaadi MA, Julkapli NM, et al. (2019) Hybrid nanocomposite curcumin-capped gold nanoparticle-reduced graphene oxide: Anti-oxidant potency and selective cancer cytotoxicity. PLoS ONE 14(5): e0216725. https://doi.org/10.1371/journal.pone.0216725

Editor: Yogendra Kumar Mishra, Institute of Materials Science, GERMANY

Received: January 22, 2019

Accepted: April 28, 2019

Published: May 14, 2019

Data Availability Statement: All relevant data are within the manuscript and its Supporting Information files.

Funding: This study was funded by University Malaya Research Grant UMRG [RP044C-17AET] – University of Malaya, Malaysia, received by W.A. Yehye. The project was further supported by South Asia Taiwan Universities SATU grant [ST018-2017] received by W.A. Yehye. The funding sources had no role in study design, data collection and

Abstract

Nanotechnology-based antioxidants and therapeutic agents are believed to be the next generation tools to face the ever-increasing cancer mortality rates. Graphene stands as a preferred nano-therapeutic template, due to the advanced properties and cellular interaction mechanisms. Nevertheless, majority of graphene-based composites suffer from hindered development as efficient cancer therapeutics. Recent nano-toxicology reviews and recommendations emphasize on the preliminary synthetic stages as a crucial element in driving successful applications results. In this study, we present an integrated, green, one-pot hybridization of target-suited raw materials into curcumin-capped gold nanoparticle-conjugated reduced graphene oxide (CAG) nanocomposite, as a prominent anti-oxidant and anti-cancer agent. Distinct from previous studies, the beneficial attributes of curcumin are employed to their fullest extent, such that they perform dual roles of being a natural reducing agent and possessing antioxidant anti-cancer functional moiety. The proposed novel green synthesis approach secured an enhanced structure with dispersed homogenous AuNPs (15.62 ± 4.04 nm) anchored on reduced graphene oxide (rGO) sheets, as evidenced by transmission electron microscopy, surpassing other traditional chemical reductants. On the other hand, safe, non-toxic CAG elevates biological activity and supports biocompatibility. Free radical DPPH inhibition assay revealed CAG antioxidant potential with IC_{50} (324.1 ± 1.8%) value reduced by half compared to that of traditional citrate-rGO-AuNP nanocomposite (612.1 ± 10.1%), which confirms the amplified multi-potent antioxidant activity. Human colon cancer cell lines (HT-29 and SW-948) showed concentration- and time-dependent cytotoxicity for CAG, as determined by optical microscopy images and WST-8 assay, with

analysis, decision to publish, or preparation of the manuscript.

Competing interests: The authors have declared that no competing interests exist.

relatively low IC_{50} values (~100 μg/ml), while preserving biocompatibility towards normal human colon (CCD-841) and liver cells (WRL-68), with high selectivity indices ($\geq$ 2.0) at all tested time points. Collectively, our results demonstrate effective green synthesis of CAG nanocomposite, free of additional stabilizing agents, and its bioactivity as an antioxidant and selective anti-colon cancer agent.

Introduction

Among the various nanomaterials reported to date, graphene has ascended as the 'wonder material' and 'shining star', with a Nobel Prize awarded in 2010 for its discovery [1]. Due to the interesting chemical, mechanical, and optical properties, graphene applications have been actively pursued in the general biomedical fields, with distinctive focus on cancer nanomedicine, to confront the increasing cancer mortality rates [2–7]. In this context, graphene offers a range of nano-therapeutic modalities of phototherapy, drug delivery, and combination therapy [8–10]. This enables efficient support for functionalization and drug loading [11, 12], in addition to enhanced mechanical stability and cellular interactions [13]. The few limitations of graphene such as hydrophobicity and self-aggregation, can be effectively resolved via suitable functionalization and composite hybrid fabrication [14]. In fact, various studies have proven advantageous attributes using graphene-based composites (GBCs) in cancer nano-therapy, over raw un-functionalized graphene counterparts [15–17]. Nevertheless, the progress and development of these composites to the next *in vivo* and clinical stages remains slow [12]. The main barrier recognized is the safety profile, or biocompatibility and selectivity, of these composites towards normal tissue [12, 13]. After all, drug selectivity and enhanced patients' life quality are the ultimate goal of nanotechnology in cancer treatment [18, 19].

For successful and selective cancer nano-therapy applications, more attention needs to be directed to GBCs fabrication and pre-clinical trials, as these processes constitute the basic foundation for further development and progress. In fact, careful design and suitable choice of raw materials and synthesis methodology are suggested approaches to increase GBCs biocompatibility [13, 20]. Accurate reporting of the selectivity index (SI) in pre-clinical *in vitro* testing is also an important factor determining safety and indicating successful employment of raw materials in cancer-active, normal cell-biocompatible composites. As such, current nanomedicine research indicates that graphene selection as a starting build-up template secures essential planar surface area that is suitable for functionalization and drug upload [21]. On the other hand, gold nanoparticles (AuNPs) stand out as a prominent functional moiety used heavily with various nanomaterials [11, 22], due to the stable [23], well-established biocompatible features that enhance the overall composite selectivity [11, 24]. Consequently, graphene-AuNPs hybrid composite is one of the best-studied materials in the field of cancer nano-therapy [25–29]. Furthermore, there is a mounting focus devoted to the hybridization and synthesis methodology used to combine different moieties into one nanocomposite. Green synthesis is recently identified as an easy, eco-friendly, cost-effective, safe, and efficient alternative to conventional chemical synthesis, further reinforcing biological activities of the whole system [30, 31]. As a result, there are various reports of GBCs synthesized by green methods (S1 Table), yet the majority show inconsistent use of human cancer/normal cell lines, with a lack of SI reporting in respective target tissues, which may contribute to indeterminate conclusions and hinder further development [13].

Apart from synthesis approaches, the suitable anti-cancer drug incorporation holds fundamental values and merits. Plant-derived drugs account for over 60% of drugs introduced worldwide recently [32], including *Curcuma longa* polyphenolic extract curcumin (CR), which

has been the focal point of modern cancer research [33, 34]. Its major advantage lies in its multi-targeted therapeutic approach, which is of utmost importance to confer cancer disease that holds more than 500 gene products dysregulation [34, 35]. The astonishing ability of CR to inhibit tumor proliferation, cell cycle, metastasis, and angiogenesis is limited by its low bioavailability [34, 35]. Therefore, CR nano-formulations are prescribed as a valid solution [36]. In this study, we suggest, for the first time, the one-pot combination of all these beneficial attributes of graphene, AuNPs, and CR into one novel green nanocomposite, namely CR-capped AuNPs-reduced graphene oxide (CAG). Unlike previous reports of CR combining with GBCs through two-step chemical reactions [37, 38], this work proposes a novel green, simple, one-pot synthesis which uses CR to its fullest potential as a natural reducing agent, with capping and functionalization moiety during synthesis, while also preserving its anti-oxidant, cancer cytotoxic, and selective biological activities. This structure is anticipated to confer superior features, overcoming the limitations faced by each single component, in addition to being a green and safe product with no toxic impurities and increased biocompatibility. Comprehensive *in vitro* cancer cytotoxicity and respective selectivity indices are discussed in the current work, in terms of various concentrations, time points, and cell lines chosen to represent suitable target colon cancer tissue and distant normal liver cells, which mimic the probable *in vivo* behavior of GBCs as reported previously [39, 40]. We believe, as recommended by nano-toxicology reviews [41], that careful design and accurate SI measurement will improve knowledge gathered at the preliminary *in vitro* stage, creating a worthwhile template eligible for various biomedical applications and further study and development.

Materials and methods

Nanocomposite synthesis

GO synthesis. Graphite oxide was prepared using the 'improved Hummer's method', as reported previously [42]. In brief, 1.0 g of graphite powder (Sigma Aldrich, < 20 μm) was mixed with 135 mL of 9:1 mixture of sulfuric to phosphoric acid, followed by slow addition of 6.0 g of potassium permanganate. The reaction mixture was then heated to 50˚C and maintained in stirring conditions for 12 hours. The mixture was brought to room temperature and poured on iced deionized (DI)-water. In order to stop the reaction, dropwise addition of 30% hydrogen peroxide was performed, and a color change to yellow was observed. The yellowish suspension was then processed by multiple centrifugation and washing steps with DI-water, 30% HCl, ethanol, and DI-water again. The final pellet was dialyzed against DI-water using a dialysis membrane for 48 hours, and freeze dried.

CAG nanocomposite synthesis. The prepared graphite oxide powder was dispersed in DI-water and sonicated for 30 minutes in a bath sonicator to exfoliate sheets into graphene oxide (GO). The solution was then added to $HAuCl_4$ solution (Sigma Aldrich), and aged for 30 minutes to promote gold ion attachment to the GO surface [43]. The mixture was then heated at 80˚C, before CR solution was added (Merck, Germany). CR was first dissolved in DMSO, used as a stock solution, and then diluted with DI-water to give a 1 mM working solution. The pH of CR was adjusted (~9.0) with a weak base (sodium bicarbonate) prior to addition. After mixing all solutions in the flask, the reaction was kept at 80˚C for 4 hours under stirring conditions. Later, the solution was brought to room temperature, and wash-spinned with DI-water several times to remove excess gold ions and control pH at ~7.0. The CAG pellet was finally obtained via freeze drying.

For comparison purposes, the rGO-AuNPs nanocomposite was synthesized by the traditional sodium citrate reduction method [43], and citrate-AuNPs were synthesized as described previously [44].

Morphological and structural characterization

The synthesized materials were morphologically characterized by high resolution transmission electron microscopy (HR-TEM, Hitachi-HT7700, 120kv, Japan) to investigate the sheet-like morphology of rGO, and the formation of AuNPs and their size and dispersion patterns. A few drops of each sample were allowed to air-dry on a lacy copper grid coated with carbon film for TEM analysis. Graphene structural features were revealed using Raman spectroscopy (Renishaw inVia Raman, Gloucestershire, UK) with a 514 nm argon gas laser. Fourier-transform infrared spectroscopy (FT-IR) analysis was performed to detect functionalization, wherein the sample powder was ground with potassium bromide (KBr) into thin pellets. FT-IR spectra were recorded using a Spectrum 400 (PerkinElmer, Boston, MA, USA). X-ray diffraction patterns (XRD) were recorded using an EMPYREAN diffraction system with X-ray wavelength of 1.54060 Å. UV-Vis spectroscopic measurements were performed using PerkinElmer–Lambda 35 spectrophotometer at a wavelength range of 200–800 nm. Thermo-gravimetric analysis (TGA) was performed using a TGA/SDTA 851 (Mettler Toledo, USA) system with a heating rate of 10˚C/min up to 800˚C in a nitrogen environment. Dynamic light scattering (DLS) of CAG nanocomposite in cell culture RPMI-1640 medium was analyzed using Zetasizer Nano-ZS apparatus (Malvern Instruments, UK) at 25˚C.

Phenol content and anti-oxidant activity

To explore the presence of possible bioactive phenol moieties and the anti-oxidant activity of the CAG nanocomposite, total phenolic content (TPC) and DPPH (2,2-diphenyl-1-picrylhydrazyl) anti-oxidant tests were performed. TPC was measured using improved Folin-Ciocalteu (FC) protocol as described previously [45]. Briefly, 50 μL FC reagent (1:5 (v/v)) was mixed with 50 μL of sample in a 96-well plate (Nest Biotechnology, China). NaOH (0.35 M; 100 μL) was then added to the mixture and incubated for 3–4 minutes in the dark. Results were read at 760 nm absorbance of a microplate reader (Infinite-200Pro-TECAN). Ethanolic CR solution was used to create the standard calibration curve [46].

The anti-oxidant activity of the composite was evaluated using optimized DPPH assay [47, 48]. Ascorbic acid was used as a positive control in this experiment, while methanol served as a blank. Methanolic DPPH stock solution (2,2-diphenyl-1-picrylhydrazyl, Sigma-Aldrich) was prepared to yield a final concentration of 70 μM upon addition to sample (50–750 μg/mL). DPPH was added to all control and test tubes, followed by successive sonication (3 times, 3 minutes each, in dark) during 30 minutes of incubation. Absorbance was read at 517 nm using a microplate reader (Infinite-200Pro-TECAN). The percentage inhibition was calculated using Eq (1), where Abs. stands for absorbance measured at 517 nm:

$$\%\ inhibition = (Abs.Control - Abs.Sample)/Abs.Control\ x\ 100 \quad (1)$$

To determine IC_{50} values (sample concentration required to achieve 50% inhibition) of the DPPH radical, the percentage inhibition for each compound was plotted against different concentrations.

Cell-based assays

Cell culture. Human colon cell lines HT-29 (colon adenocarcinoma), SW948 (Duke's C colorectal carcinoma) and CCD841-Con (normal colon cells), in addition to human liver WRL-68 (normal hepatic cells) were all obtained from American Type Culture Collection (ATCC, Manassas, USA). Cells were cultured in RPMI-1640 medium (Sigma Aldrich, USA), supplemented with 10% fetal bovine serum (Gibco, USA), and 1% Pen-Strip antibiotic (10,000

units penicillin-10 mg streptomycin/mL, Sigma Aldrich, USA) in a 37˚C, 5% CO_2 incubator (Thermo Fisher Scientific, USA).

Cell Morphology using optical microscopy imaging. Cancer cells' morphological changes upon nanocomposite exposure were observed using phase-contrast optical microscopy. Cells were plated in 24-wells plate (5 x 10^4 cells/ml) and incubated overnight for attachment. Culture media was then removed and replaced with CAG suspension in media at low concentration (62.5 μg/ml) and high concentration (250 μg/ml) for 24 hours. Untreated cells were used as control, while treatment with raw material GO and traditional synthesized nanocomposite rGO-AuNPs were used for comparison. Phase-contrast bright field images were recorded via inverted microscope Eclipse Ti-S (NIKON Instruments, USA).

Cellular viability assay using WST-8. Cellular viability was assessed in CAG-treated cancer and normal cells using water soluble tetrazolium test (WST-8). Cell counting kit-8 (CCK-8, Sigma Aldrich, USA) was applied following the manufacturer's protocol. Typically, 5000 cells were seeded in 96-well plates and incubated overnight for attachment. Following that, the medium was removed and cells were treated with 100 μL of different concentrations of CAG suspensions in media. After each time point (24, 48, and 72 hours), 10 μL of CCK-8 solution was added to each well, and incubated for a further 4 hours at 37˚C, 5% CO_2. At the end of incubation period, 80 μL was transferred from each well to a new 96-well plate, to avoid residual CAG precipitate that may affect absorbance readings [49]. The test was conducted in triplicate. Results were recorded using 450 nm absorbance value by (Infinite-M200Pro-TECAN). The percentage cell viability was calculated according to Eq (2):

$$Cell\ viability\ (\%) = Sample\ Absorbance/Control\ Absorbance\ x\ 100 \quad (2)$$

For comparison purposes, WST-8 test was performed as well using GO and rGO-AuNPs following the same assay conditions.

Selectivity index (SI). The degree of selectivity of composite to the cancer cell line is explored as SI ratio as per previous reports [50, 51], according to the following Eq (3):

$$SI = IC50\ composite\ on\ normal\ cell\ line/IC50\ composite\ on\ cancer\ cell\ line \quad (3)$$

Statistical analysis. Numerical results were expressed as the mean ± standard error of the mean (SEM) from triplicate experiments. Statistical significance was determined using factorial analysis of variance (ANOVA) test, with p value set at < 0.05 as accepted level of significance. All analyses were performed using SPSS software (Statistical Packages for Social Science, version 22.0, IBM Corporation, NY, USA).

Results and discussion

Integrated hybridization with multi-functional approach

One of the promising concepts behind nanotechnology is hybridization, the remarkable outcome of which is a composite that merges various moieties, producing superior features with enhanced performance. For that reason, a novel, hybrid, and green incorporation of valuable well-studied nanomaterials of graphene, AuNPs, and natural CR into one nanocomposite is proposed as a multi-functional biocompatible agent, turning previous limitations into advantages. As illustrated in Fig 1, graphene in a CAG structure works as a template with a high planar surface area for maximal upload of AuNPs and the anti-cancer drug CR [11, 12]. The lipophilic nature of graphene is of major significance, ensuring cellular uptake and thus delivery of treatment cargo into cancer cells, surpassing membrane-penetration obstacles [12, 52], and low CR bioavailability and absorption deficiency [53]. On the other hand, AuNPs as a functional tool acts as a spacer preventing

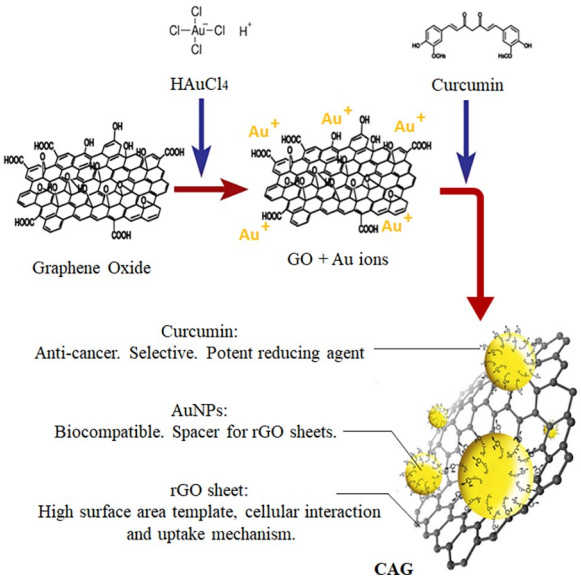

Fig 1. CAG nanocomposite synthesis illustration.

https://doi.org/10.1371/journal.pone.0216725.g001

graphene sheet aggregation, which would adversely affect cellular viability and colloidal stability attributes [54]. The biocompatible nature of core gold also adds to the selectivity profile of the whole system [55, 56]. Curcumin outstandingly serves dual roles in the synthesized CAG nanocomposite as an anti-cancer drug and a potent green reducing agent for simultaneous gold salt and GO reduction and composite fabrication. This synthesis approach skipped the conventional use of chemical stabilizers or capping agents needed for stable unaggregated AuNPs formation [43, 57], thus providing a novel green nanocomposite free of chemical waste and impurities that may support cross-chemical effects [57–60]. Indeed, plant-derived green synthesis is not only preferred over chemical routes, but also comes first in the hierarchy of biological synthetic approaches, as it eliminates cost/time/effort exhaustion in preserving bio-cultures for large scale production [61]. In total, suitable raw materials were integrated by a novel, green, impurity-free synthesis approach, for a multi-functional hybrid with complementary advanced features.

The expected mechanism behind CAG synthesis is explained initially by the opposite charge attraction between oxygen functionalities of GO and Au^{3+} ions in solution [62], followed by reduction in-place to form AuNPs via CR action [62]. The alkaline pH together with the suitable molar ratio were applied based on previous optimization studies to ensure CR peak reduction [63]. The resulting CR anions are expected to be the ingredient responsible for the reduction. This mechanism is thought to progress through six stages, as explained by Sindhu et.al (2014), using CR in nano-synthesis. The stages extend for 4 hours and include deprotonation of CR, gold ion reduction, nucleation, growth, cleavage, and finally, maturation [63]. AuNPs is expected to be stabilized by ionized CR molecules on the CAG surface. Fig 2 represents the possible reduction sites of Au ions by CR as concluded and reported previously [63]. Characterization results, as explained below, collectively confirm this mechanism and assure successful utilization of CR as a powerful reducing and capping agent.

Morphological and structural features

Transmission electron microscopy (TEM) images (Fig 3) clearly show the successful synthesis of nanocomposite rGO-AuNPs using CR to yield CAG. This synthetic route was compared to

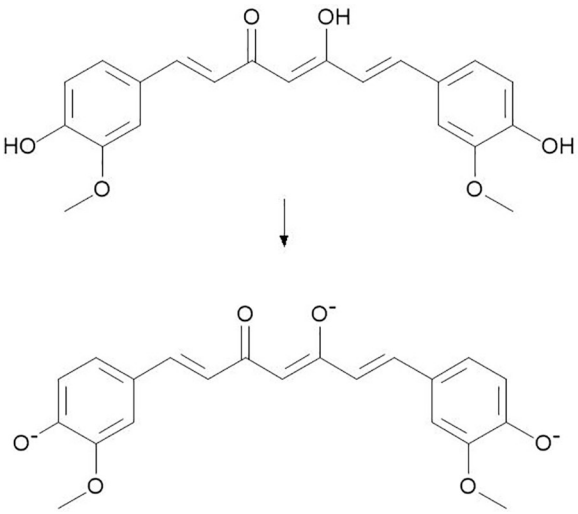

Fig 2. The proposed reduction sites action of CR. The O^- moieties formed at alkaline pH are assumed to reduce Au^+ ions to AuNPs [63].

https://doi.org/10.1371/journal.pone.0216725.g002

traditional *in-situ* reduction synthesis of an rGO-AuNP composite using sodium citrate [43]. Both images displayed the typical sheet-like morphology of graphene; however, the morphology of AuNPs anchored to the surface differs significantly. As shown, AuNPs are well-dispersed, with nearly uniform and homogenous spherical shape and size (15.62 ± 4.04 nm), using CR as the reducing and capping agent in the CAG composite. On the other hand, citrate produced aggregated AuNPs on the rGO surface. This finding is in agreement with previous studies that report aggregated AuNP formation on the rGO surface because of weak citrate function as a capping agent [43]. The mechanism of AuNP aggregation was explained by Chuang et.al (2014), as free-standing AuNPs formed in solution displace citrate ions, which weakly cap anchored AuNPs on the rGO surface. This leads to the formation of chain-like aggregated AuNPs [43]. The TEM results indicated that CR not only reduces gold salt to AuNPs, but also provides a strong capping and stabilizing action to the formed AuNPs on the

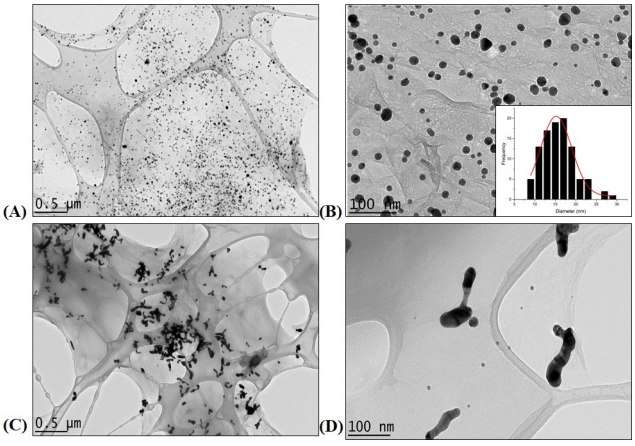

Fig 3. TEM images of CAG vs. rGO-AuNP nanocomposites. (A) CAG composite at 0.5 μm scale, (B) CAG at 100 nm scale with an inset of size distribution histogram. (C) rGO-AuNPs prepared using sodium citrate at 0.5 μm scale, (D) rGO-AuNPs at 100 nm scale.

https://doi.org/10.1371/journal.pone.0216725.g003

rGO surface, preventing their aggregation without the need to add additional chemicals as used previously [43]. The remaining AuNPs in solution can be easily removed by washing and purification steps followed in the synthesis protocol [43].

Raman spectroscopy is a potent technique to reveal graphene structural changes upon functionalization [64–67]. In general, graphene-based composites exhibit characteristic G bands (1580 cm^{-1}) indicative of sp^2-hybridized carbon atoms stretch, and G' bands (2500–2800 cm^{-1}) [65, 66]. A Raman spectrum was recorded for CAG nanocomposite in comparison with raw materials used in the synthesis of graphite and GO, as shown in Fig 4. Both G and G' bands appeared in all tested composites, which assures a preserved graphitic template after functionalization reaction with AuNPs and CR. On the other hand, a disorder-induced D band in GO and CAG nanocomposite spectra refers to sp^3-hybridized carbon systems, resulting from the functionalization out of raw pure graphite [66]. The novel nanocomposite CAG spectrum revealed upshift in bands position (G and D bands at 1605, and 1358 cm^{-1}), compared to graphite (1581, 1352 cm^{-1}) and GO (1600, and 1351 cm^{-1}), respectively. This further confirms AuNPs interaction and doping on graphene surface [68, 69]. Additionally, the enhanced intensity values observed in CAG spectrum reflects surface enhanced Raman resonance (SERS) effect, as reported previously for AuNPs-functionalized-graphene composites [68, 70].

The intensity ratio I_D/I_G is commonly reported to assess the sp^2 domain extent in graphene composites [65]. The starting material GO scored a ratio of 0.86, while it reached 0.85 for CAG

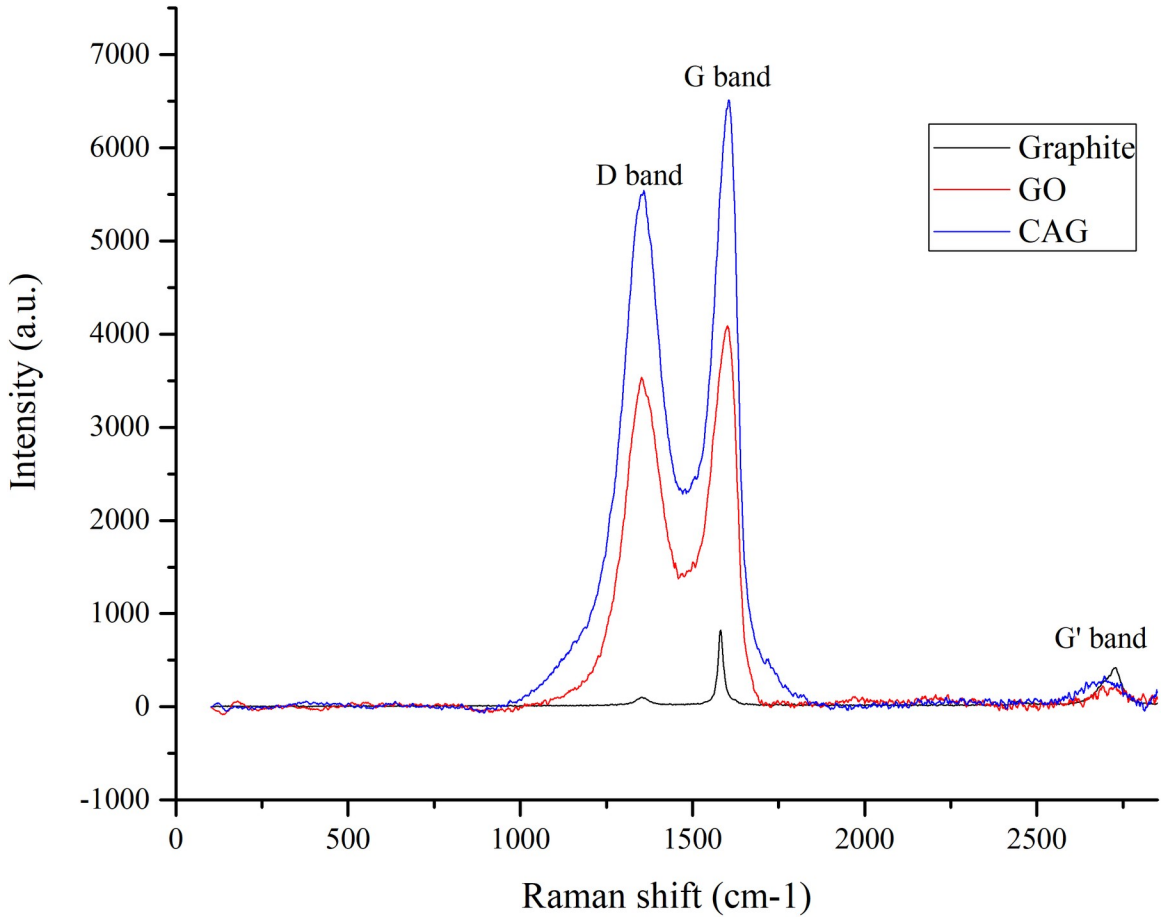

Fig 4. Raman spectra of synthesized nanocomposite CAG, GO and graphite.

https://doi.org/10.1371/journal.pone.0216725.g004

nanocomposite. The slight decrease in ratio marks partial reduction of GO to rGO by CR action [43, 65, 71], which is consistent with the reducing nature of CR, and its interaction with some oxygen functionalities of GO [43, 64].

The presence of the functional group, including CR moieties attached to the CAG surface, was studied by Fourier transform infrared spectroscopy (FT-IR). Fig 5A presents the FT-IR spectra of the CAG composite compared to GO and CR. The GO spectrum shows multiple peaks that correspond to different O_2-functional groups. The most intense peaks at 2857 and 2923 cm^{-1} represent methyl C-H bond for graphene structure [72]. Other prominent peaks at 1027 cm^{-1}, 1096 cm^{-1}, and 1260 cm^{-1} reflect absorbance intensities of carbon-oxygen (C-O) bonds [65]. However, some of these peaks disappeared or appeared with only weak absorbance in the CAG composite, which indicates reduction to rGO by curcumin action. Herein, CAG exhibited a reduced graphene pattern as cited in previous studies, whereby O_2 functional groups appeared at 1090 cm^{-1} (C-O stretch) but with low intensity [73, 74], as well as peaks at 1576 cm^{-1} corresponding to C = C [64]. However, additional fingerprint peaks were observed at 1026 cm^{-1}, 1099 cm^{-1}, and 1263 cm^{-1}, indicating curcumin presence in its intact form with bonds of (C-O) and carbonyl (C = O) at 1625 cm^{-1} [63–65]. By comparison with a pure curcumin spectrum, the multiple peaks at a range of 1028–1510 cm^{-1} appeared as well in the CAG composite, which in turn confirms the successful interaction of CR with graphene and gold [63, 64]. The bands observed at 1265 cm^{-1}, 1384 cm^{-1}, and 969 cm^{-1} in the CR spectrum reflect hydroxyl stretches of phenolic and enolic groups, respectively. These bands appeared with only low intensities in CAG, which may explain the interaction sites of CR to Au on the rGO surface [63], as explained and illustrated earlier in text (Fig 2).

To confirm the successful formation and attachment of AuNPs to the rGO surface, X-ray diffraction (XRD) analysis was used, which further helps to explore the crystalline structure of the composite. Fig 5B shows XRD patterns of CAG in addition to GO, which served as a precursor for synthesis. As shown, GO had a characteristic XRD pattern with an intense peak at 10˚C (2θ), which corresponds to the crystalline orientation of (001) and d-interlayer spacing of ~0.88 nm due to oxygen-functionalized groups exfoliating carbon sheets [42, 64, 75, 76]. In contrast, the 10˚C peak was significantly decreased in intensity in the CAG diffractogram, indicating reduction of oxygen-groups into rGO and restoring the graphene sp^2 network, giving a characteristic feature of a broad peak at 22.12˚C [64, 74, 77]. Formation of AuNPs can be determined by the presence of 2θ peaks at around 38˚C, 44.3˚C, 64.7˚C, and 77.7˚C, corresponding to the formation of pure metallic gold with crystal faces (111), (200), (220), and (311), respectively [74, 77]. These peaks were observed in the CAG nanocomposite,

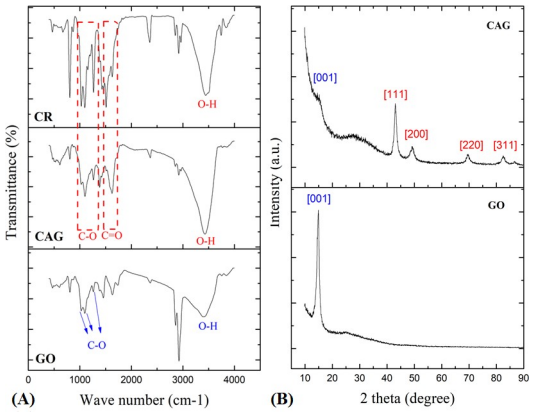

Fig 5. FTIR and XRD analysis. (A) FT-IR spectra of GO, CAG, and CR. (B) XRD analysis of GO and CAG.

https://doi.org/10.1371/journal.pone.0216725.g005

confirming the anchoring of AuNPs on the rGO surface through functionalization [74]. Collectively, it has been proven that CR successfully played dual roles in CAG synthesis, reducing both gold salt into AuNPs, and also GO into rGO sheets.

Additional confirmatory results of CAG structural features discussed earlier can be obtained through UV-Vis absorption analysis (Fig 6). Typically, GO exhibits an absorption peak at around 235 nm with a weak shoulder at around 310 nm due to C = C and C = O bonds, respectively [42, 64, 78]. On the other hand, AuNPs shows a dominant absorption peak at 520 nm [44, 79]. The CAG nanocomposite UV-Vis pattern revealed a shifted peak of GO into ~255 nm absorption wavelength, which indicates the reduction process of GO into rGO by CR action [64, 65]. Formation of AuNPs on the CAG surface is confirmed by the presence of a 540 nm absorption peak [63]. The peak shift from 520 to 540 nm is reported as a confirming indicator for the deposition of Au on graphene sheets [74]. Furthermore, a CR prominent absorption peak observed at 430 nm disappeared upon mixing with the CAG composite, denoting chromophore interaction with the rGO surface [64].

Functionalization on the carbonaceous nanocomposite surface can be also examined by thermogravimetric analysis (TGA) [64]. Fig 7 shows TGA curves under nitrogen gas flow for CAG in comparison to graphite, GO, and CR. Raw graphite demonstrated high thermal stability with no weight loss over the entire temperature range [64, 80]. On the other hand, functionalized graphene composites in this study showed multi-stage decomposition patterns. GO

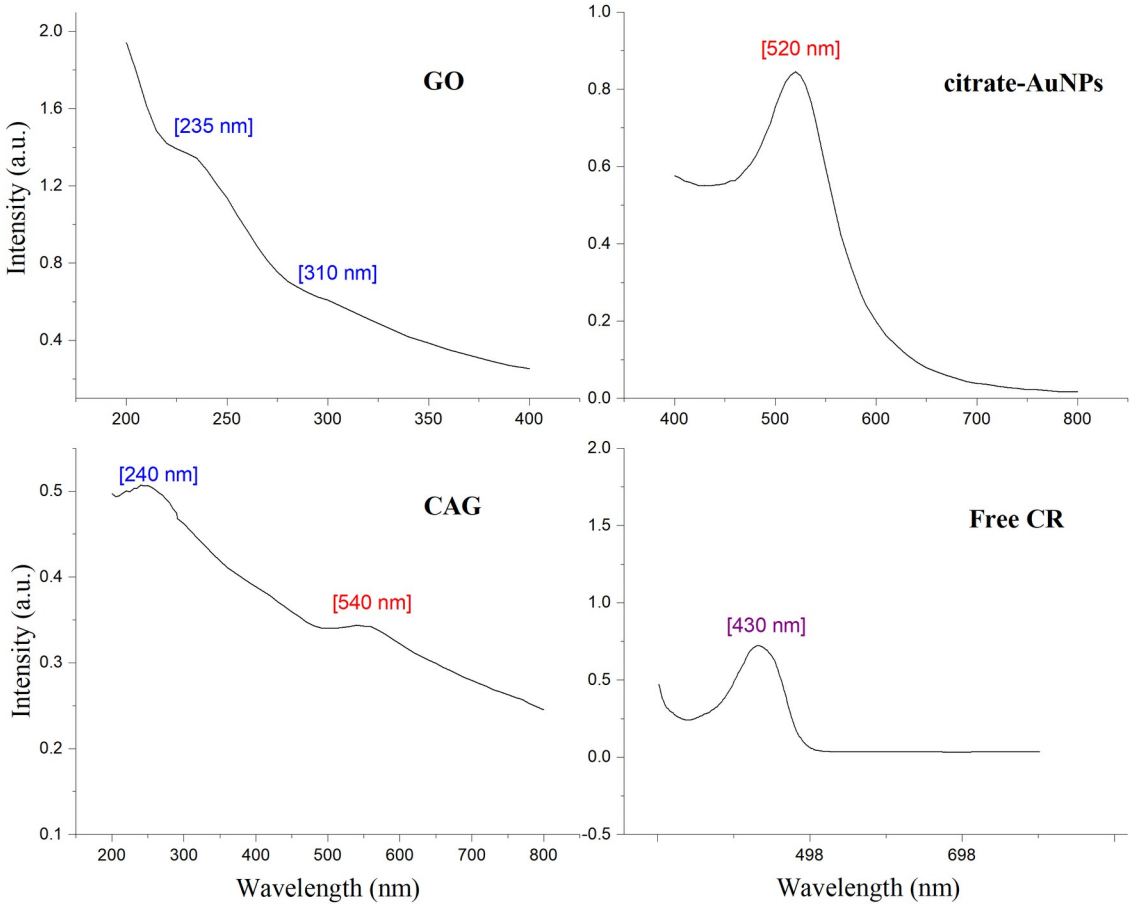

Fig 6. UV-Vis absorption spectra. Panel of GO, citrate-AuNPs, CAG, and CR.

https://doi.org/10.1371/journal.pone.0216725.g006

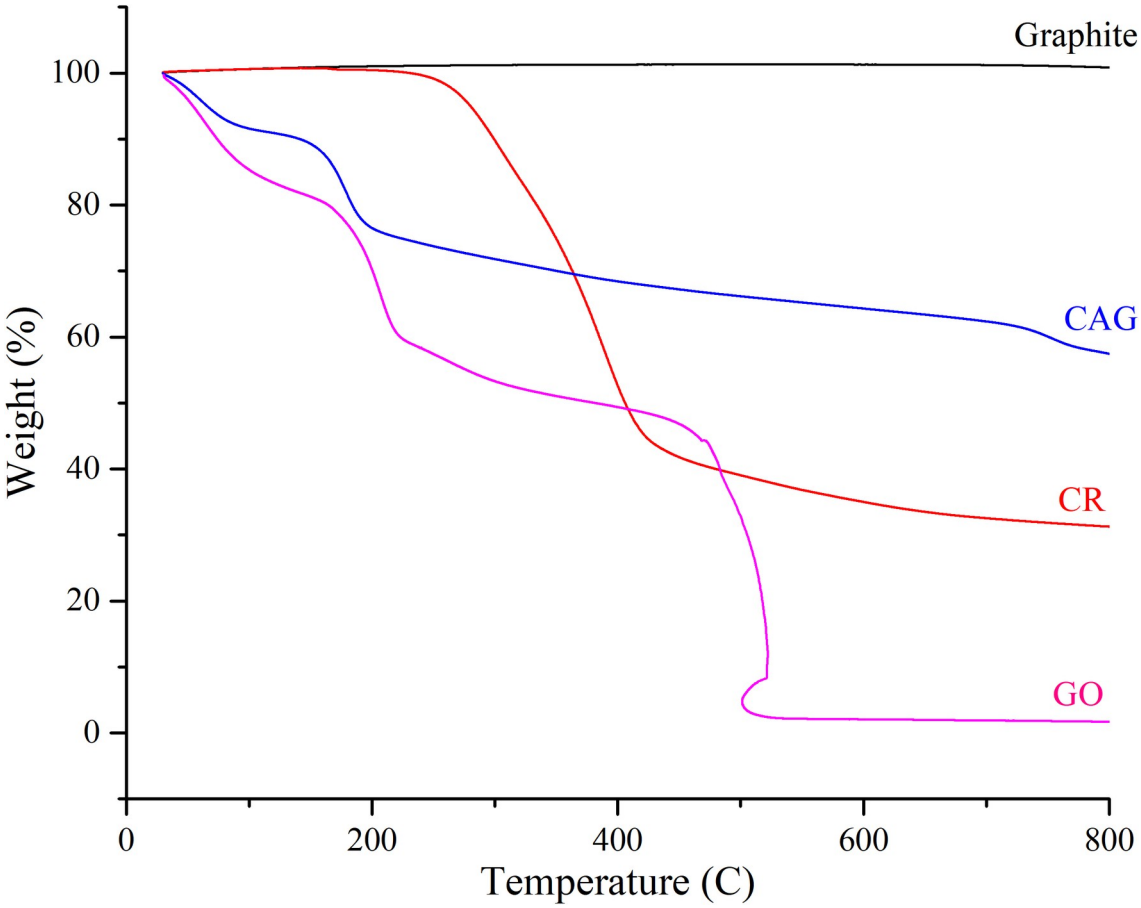

Fig 7. TGA curve trends. TGA curves for CAG in comparison to graphite, CR, and GO.

https://doi.org/10.1371/journal.pone.0216725.g007

thermal degradation can be classified into 3 stages, the first weight loss of ~19.5% occurred at temperature 159˚C, attributed to water evaporation. The second weight loss of 52.5% occurred at temperature range 159–440˚C, related to the removal of oxygen-functional groups. The final stage at 440–528˚C left residual weight of only 2.3%, due to combustion and formation of carbon dioxide [64, 81]. The commercial curcumin TGA trend exhibited the signature thermal stability curve [64]. The two mass losses occurred at 240˚C and 435˚C, reflecting the removal of oxygen groups and combustion, respectively. The novel nanocomposite CAG displayed a similar TGA curve to that of GO, but with a lower weight loss rate, confirming the reduced nature of graphene in the nanocomposite, in agreement with rGO TGA trends seen in literature [80–82]. Additionally, CAG exhibited a multi-staged curve as seen in both GO and CR. A modest weight loss of 9.7% occurred at 136˚C, which can be attributed to water removal. Followed by a steep drop in weight percentage until 200˚C with total loss of 23.5%, which is thought to be related to the removal of oxygen functional groups of CR attached to the composite surface, where a similar trend was observed in previous studies utilizing CR in nanosynthesis [64]. The final gradual weight loss began at over 200˚C, with residual materials of 58.7% and 41.3% weight loss. Thus, the TGA trend of CAG nanocomposite has confirmed the reduced nature of GO [80–82] parallel with the successful functionalization of CR on the surface, which collectively increased the thermal stability compared to GO [64, 65].

Aiming for biological, anti-cancer applications require understanding of nanocomposite's bio-physical characteristics [83]. Dynamic light scattering enables measuring particles'

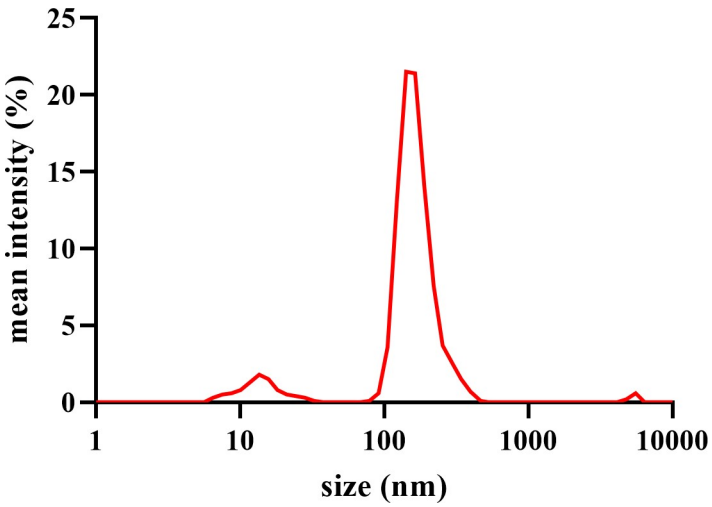

Fig 8. Dynamic light scattering. Particle size distribution of CAG nanocomposite dispersion in RPMI-1640 medium.

https://doi.org/10.1371/journal.pone.0216725.g008

hydrodynamic size distribution in biological medium, which is vital to assess dispersion stability [56, 83]. Fig 8 displays the average hydrodynamic diameter of CAG in RPMI-1640 medium (171.3 ± 30.3 nm). The presence of low-intensity peaks at different size regions represents a common finding reported in previous studies working on GBCs, due to sheet-like structures effect on DLS system that is best suited for circular particles [84–87].

Anti-oxidant activity

CR is well known to exhibit a strong antioxidant activity, as evidenced by previous *in vitro* and *in vivo* studies [35, 88–92], which correlate with its anticancer and chemo-preventive actions [93]. Thus, it is anticipated that hybridization of CR with rGO-AuNP nanocomposite will yield superior anti-oxidant potential. Free radical inhibition assessment is currently well-established procedure for nano-synthesized systems intended for biological applications, providing a critical preliminary indication for composite function and activity [94–96]. The nanocomposite CAG was investigated for anti-oxidant properties using 2,2-diphenyl-1-picrylhydrazyl (DPPH) free radical scavenging assay. Furthermore, the raw material used in synthesis–GO, and the traditionally fabricated citrate rGO-AuNPs composite were analyzed as well, for the sake of obtaining a better understanding of the CR effect added to the hybrid system. The anti-oxidant activity exerted by CAG on DPPH free radicals follows a concentration-dependent manner, as displayed in Fig 9, with obviously amplified inhibition rates compared to raw GO and citrate-rGO-AuNPs at all tested concentrations. The IC_{50} values were determined as 324.1 ± 1.8, 612.1 ± 10.1, and above 750 μg/mL (mean ± SEM) for composites CAG < citrate-rGO-AuNPs < GO, respectively. Standard antioxidant ascorbic acid as positive control along with free curcumin validated the assay results obtained (IC_{50} = 4.53 ± 0.05 and 6.84 ± 0.15%, respectively [97, 98] (S1 Fig). The observed trend suggests that CR incorporation in the nanocomposite was key for tremendous anti-oxidant enhancement, which effectively reduced the IC_{50} value approximately by half, compared to that of the rGO-AuNP traditional composite.

The proposed mechanism by which the nanocomposite CAG acts on DPPH is thought to depend on CR moiety, and to a lesser extent on AuNPs, rather than rGO. In the current experimental results, GO as a raw material was relatively inactive, with the highest concentration inhibiting less than 30% of the free radicals. The addition of AuNPs through sodium citrate conventional synthesis method enhanced the anti-oxidant activity. However, remarkable

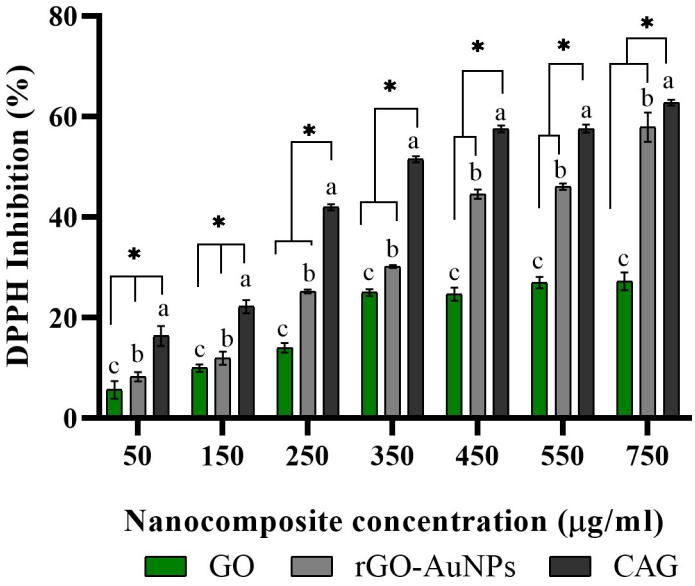

Fig 9. DPPH antioxidant assay. CAG antioxidant activity compared to raw material GO, and citrate synthesized rGO-AuNPs nanocomposite. Results expressed as mean from triplicate analysis ± SEM. [a, b] and [c] indicates a significant increase in DPPH inhibition of respective treatments (CAG, rGO-AuNPs, and GO, respectively) compared to no treatment control ($p<0.05$). * Significant difference between treatment groups at respective concentration ($p<0.05$). Statistical analysis was performed using factorial ANOVA tests, SPSS software.

https://doi.org/10.1371/journal.pone.0216725.g009

inhibition rates were achieved using CR green hybridization of GO and AuNPs. These findings correspond with existing literature demonstrating inactivity of the graphene-based family (graphene, rGO, and GO) towards DPPH free radicals, due to poor H-donation ability [99]. Furthermore, previous studies have indicated low antioxidant activity of rGO, even when prepared using green reducing agents. Spinach and clove extract were used as green reductants to prepare reduced-GO, and both scored high IC_{50} values of 1590 and 1337 μg/mL, respectively [100, 101]. On the other hand, the majority of reports confirm that AuNPs has the ability to scavenge the DPPH free radical, in consistent with our experimental result (S1 Fig) [46, 102–105]. This scavenging power is attributed to the DPPH adsorption and complex formation on AuNPs surface, which indicates the displacement of some citrate ions when sodium citrate is used in reduction [104]. In the newly synthesized nanocomposite CAG herein, it is expected that both CR and AuNPs exert radical inhibition in a multi-potent model, where CR plays the major role by its high reducing power and phenolic content, which facilitate H-donation from phenolic–OH groups to DPPH reagent [89].

Total phenolic content was determined in the CAG nanocomposite as it provides a measurement for the active functional CR on surface. The quantitative TPC was derived from a standard curve prepared from ethanolic CR solution [46], and was calculated as 7.45 ± 0.13% (w/w) (mean ± SEM from triplicate analysis) for the synthesized CAG nanocomposite. The overall antioxidant results of the CAG nanocomposite hold great promise as an efficient nano-antioxidant system with multi-potent moieties valuable for various biological and anti-cancer applications.

Colon cancer morphology, cytotoxicity and selectivity index

The strong well-known anti-oxidant and anti-cancer properties of CR have prompted the application of CAG in cancer studies, along with encouraging results from TPC and DPPH

anti-oxidant assays. The evaluation of CAG as an anti-cancer agent was studied using an *in vitro* colon cancer model through cellular morphologic changes and viability measurements. Optical phase-contrast microscopy provides an essential tool to visualize morphological changes which serve as crucial indication for treatment efficacy in inducing cell injury and death [106–108]. Viability assay, on the other hand, determines intracellular physiological capabilities and the metabolic states of treated cells. This accurate, reproducible approach constitutes the first stage of the recommended nanomaterial toxicology evaluation [109, 110]. The well-established water soluble tetrazolium assay (WST-8) was selected for its accuracy and superior detection sensitivity, which surpasses other tetrazolium reduction dyes used in cytotoxicity [111]. Its negative charge enables water soluble tetrazolium dye to be used in this experiment without interference with graphene particles, as indicated previously for MTT [49].

Colon cancer was adopted in this work to elucidate CAG effectiveness as a cancer cytotoxic agent and its selectivity indices, due to the well-suited CR and graphene properties. CR is proven to be effective against almost all cancer types *in vitro*, with colon cancer exhibiting some of the lowest IC_{50} values recorded, which indicate a high susceptibility concept. Studies have shown that deep colorectal tissues gain only around 5% of orally ingested CR [35], which is in agreement with low CR absorption and cellular uptake, and the efflux mechanisms reported from cancer cells [112–114]. These limitations create motives to design a nano-based CR hybrid that facilitates deeper penetration and delivery into colon tissues. To this end, graphene constitutes a promising platform for insoluble drug delivery [115]. Additionally, in a recent work by Lin et al. (2018), graphene oxide itself induced higher cytotoxicity towards colon cancer cells, among different panels of cancer types tested [116]. This remarkably points to a potential synergistic effect exerted by graphene and the loaded drug against colon cancer. Such approach can be termed 'design-for-purpose', which is believed to hold high potential and efficiency in applications [117–119].

Two human colon cancer cell lines were tested in this study representing different subtypes, molecular platforms, and prognosis rates: HT-29 (colon adenocarcinoma) with general good prognosis, and SW948 (Duke's C colorectal carcinoma) with poor prognosis [120]. Fig 10 demonstrates cellular changes as viewed by optical microscope upon CAG treatment. Both cell lines showed distinct size and morphology alteration compared to the untreated control. Cellular shrinkage and proliferation inhibition were observed in CAG treatment groups, which increased with higher CAG concentration, suggesting a dose-dependent trend [121, 122]. Furthermore, morphological changes were studied with starting raw material GO, and traditional citrate-synthesized nanocomposite rGO-AuNPs, as a comparative approach (S2 Fig). GO treated cells showed severe toxicity even at low concentration, which is reported previously

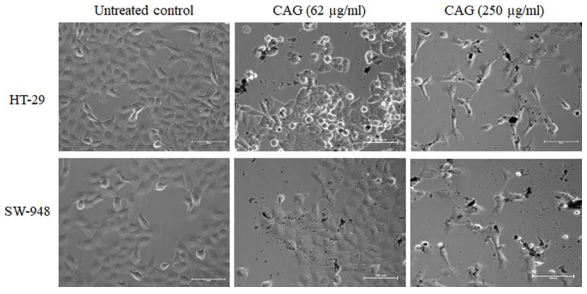

Fig 10. Optical phase-contrast microscopy images. Untreated control cells (up; HT-29, bottom; SW-948) compared to CAG nanocomposite treatment at low and high concentrations.

https://doi.org/10.1371/journal.pone.0216725.g010

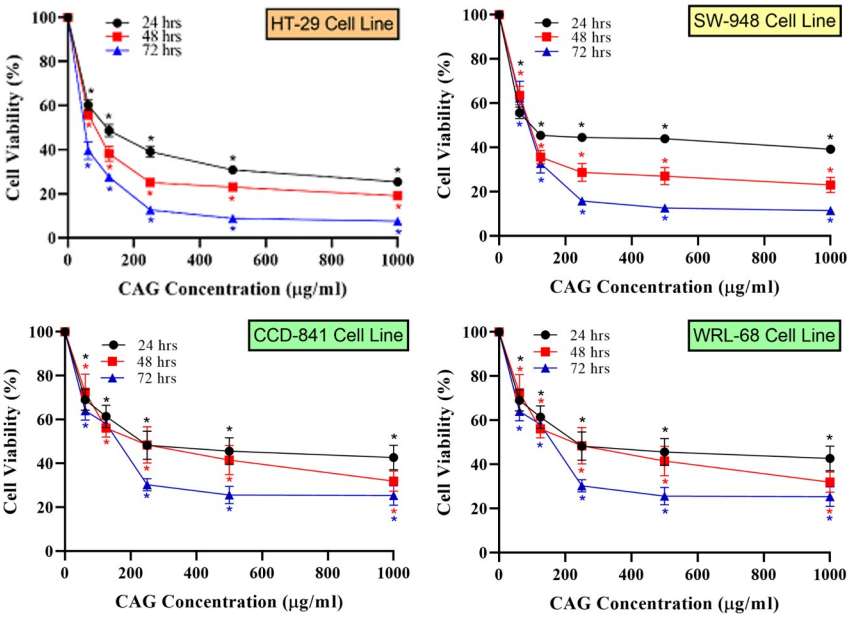

Fig 11. *In vitro* viability results after CAG treatment. Percentage viability of colon cancer cells (HT-29 and SW948 cell lines), normal colon cells (CCD841), and normal liver cells (WRL-68), upon exposure to CAG nanocomposite at different concentrations (62.5–1000 μg/mL), measured at three time points using WST-8 assay. Tests were performed and results were means from triplicate analysis. * Significant decrease ($p<0.05$) in viability percentage compared to untreated control, as analyzed by factorial ANOVA test, SPSS software.

https://doi.org/10.1371/journal.pone.0216725.g011

reflecting oxygen functionalities reactivity, that may affect GO biocompatibility in applications [115, 123]. On the other hand, rGO-AuNPs showed mild morphological changes that is less adverse than CAG, proposing the possible CR effect in CAG.

In support of the previous observations, WST-8 viability assay was conducted using various concentrations and time points. Results as presented in Fig 11, show both time- and concentration-dependent colon cancer cells inhibition in response to CAG treatment. The IC_{50} values, displayed in Table 1, demonstrate the anti-cancer effect of CAG, inhibiting 50% of cell populations at concentrations of approximately 100 μg/mL or below. These results confirm potent anti-cancer activity, which represents one of the objectives of current work. Too often, *in vitro* nano-toxicology studies would stop at this point, concluding the delivery of nanomaterial with anti-cancer properties [41]. However, a realistic optimal nano-medicine demands a broader strategy, accounting for proof of selectivity and normal cell biocompatibility, uncovering the whole picture and providing better perception of the nanomaterial under study. For that reason, parallel assessment of CAG nanocomposite on a benign cell line is conducted to accurately probe the safety profile [41]. The normal colon cell line (CCD-841) demonstrated low inhibition rates at all applied concentrations and time points. The high IC_{50} values (S2 Table) recorded for CCD-841 had proven the safety of CAG on normal colon tissue with SI

Table 1. IC_{50} values and selectivity index (SI) of cancer cells treated with nanocomposites.

	HT-29 (IC_{50} ± SEM μg/mL), SI			SW-948 (IC_{50} ± SEM μg/mL), SI		
	24 hrs.	48 hrs.	72 hrs.	24 hrs.	48 hrs.	72 hrs.
CAG	(107.8 ± 8.9), 2.1	(91.7 ± 8.0), 2.3	(59.1 ± 8.0), 2.7	(100.1 ± 8.3), 2.3	(94.0 ± 6.5), 2.2	(79.7 ± 14.2), 2.0
rGO-AuNPs	(210.8±11.1), 1.1	(149.9±17.4), 1.1	(115.3±4.5), 1.3	(151.9±16.7), 1.5	(130.6±6.1), 1.2	(101.7±16.4), 1.5
GO	(95.7 ± 9.5), 1.0	(56.3 ± 1.6), 1.2	(46.1 ± 0.5), 0.8	(72.4 ± 1.3), 1.3	(71.7 ± 2.6), 0.9	(59.6 ± 1.0), 0.6

https://doi.org/10.1371/journal.pone.0216725.t001

exceeding 2.0 –the accepted threshold for selectivity of compounds [50]–at all tested time points.

As a further verification of the integrated hybrid suggested at the introduction, the anti-cancer activity and SI were measured for GO and rGO-AuNPs as well, to confirm the superiority of green synthesis and CR functionality for drugs with cancer applications. Results were expressed as IC_{50} values and respective selectivity indices, as shown in Table 1. GO caused severe viability inhibition not only to cancer cells but also to normal cell lines, clearly evidenced through the low SI, which is consistent with morphological results explained earlier. The high O_2-functionality contents in GO can act as electron donors, causing oxidative stress-induced cytotoxicity, among other cellular damaging effects [115, 123]. In response, various strategies were recommended to minimize cytotoxicity while maintaining solubility, which includes the use of rGO instead of GO [123], as well as functionalization with biocompatible AuNPs [11, 24, 115, 124]. These factors can explain the enhanced selectivity indices of rGO-AuNPs and CAG nanocomposites seen in Table 1, reflecting the reduced graphene nature, along with AuNPs functionalization. Nonetheless, the acceptable SI was achieved only when applying CAG, distinctly manifesting the CR role and green synthesis effect with SI percentage enhancement of ≥90% for HT-29 and ≥30% for SW-948 cancer cells, compared to traditional rGO-AuNPs.

Towards comprehensive selectivity evaluation, CAG was further tested for SI in liver normal cells (WRL-68) as RES organ, standing for a possible model of CAG clearance and deposition, reported in the literature for graphene-based materials tested *in vivo* [39, 40]. We believe that this step will aid in relating to CAG behavior in a biological setting, providing an important glimpse of the suitability of nano-system design and function. Similar to colon tissue, liver normal cells showed low inhibition rates with allowable SI (S3 Table). Collectively, results obtained in this work suggests a possible interactive pathway of cells with CAG nanocomposite, as illustrated in Fig 12. The well-documented graphene-cell interaction and uptake [123]

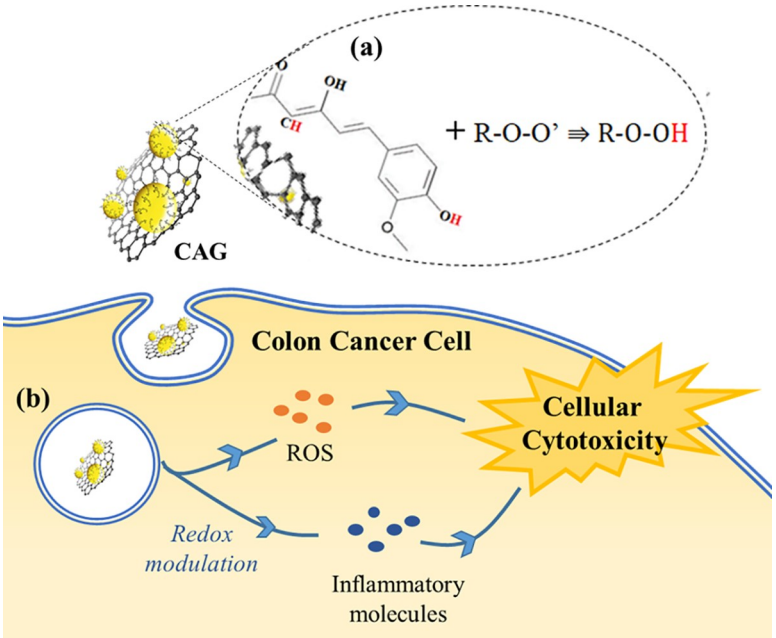

Fig 12. Schematic illustration of the proposed CAG interaction and mechanism of action on cell. (a) Antioxidant activity and free radical inhibition, (b) CAG-cell interaction and proposed subsequent mechanism.

https://doi.org/10.1371/journal.pone.0216725.g012

is proposed to facilitate subsequent intracellular activities. The nanohybrid with CR moiety effectively inhibit free radicals, as proven by DPPH assay, which is thought to be the vital key in projecting superior cancer cytotoxicity effects, through counteracting and redox modulation of the built-in high ROS and inflammatory intracellular tumor environment [125]. In fact, redox-modulation cytotoxicity symbolizes the prominent pathway for both CR-based nano-formulations, and nano-toxicology materials in general as reported in previous research [121, 126–131].

Conclusion

This study presented the novel, green, fabricated nanocomposite CAG and demonstrated its effectiveness as an antioxidant and selective anti-cancer agent. The raw material selection was driven by the individual effective features, leading to simple, one-pot, green incorporation and investment into a superior integrated hybrid system, with maximal use of CR beneficial multi-functional attributes. Characterization results demonstrate a CR functionalized structure with dispersed homogenous AuNPs with no added stabilizer, surpassing a major problem reported previously with traditional chemical reductants. Our data also showed potent anti-oxidant and anti-cancer properties with *in vitro* colon cell lines. The preserved selectivity among various tissue representatives was further proof of reliable *in vitro* nano-medicine holding great promise for further development and assessments. The sum of data reported herein strongly suggests that precise planning for nanomaterial fabrication, green synthesis, and careful selectivity measurements add much to the output nanocomposite designated for biological applications.

Supporting information

S1 Table. Examples of GBCs synthesized in previous studies by green chemistry for cancer applications.
(DOCX)

S2 Table. IC_{50} values of colon normal cell line CCD-841 treated with nanocomposites at different time points. Measurements obtained through the WST-8 assay. Results were expressed as mean ± SEM (μg/mL) from triplicate analysis.
(DOCX)

S3 Table. IC_{50} values of the liver normal cell line WRL-68 treated with the CAG nanocomposite at different time points. Measurements obtained through the WST-8 assay. Results were expressed as mean ± SEM (μg/mL) from triplicate analysis.
(DOCX)

S1 Fig. DPPH free radical inhibition assay. (a) Standard ascorbic acid, (b) free CR, (c) sodium citrate-gold nanoparticles (AuNPs). Results were expressed as mean ± SEM (μg/mL) from triplicate analysis.
(TIF)

S2 Fig. Optical microscopy images of GO and rGO-AuNPs treated cancer cell lines.
(TIF)

Acknowledgments

We would like to show our gratitude to technical staff and lab members at NANOCAT research centre, as well as the cell culture lab, pharmacy department, University of Malaya for their technical assistance and support throughout this project.

Author Contributions

Conceptualization: Lina A. Al-Ani, Wageeh A. Yehye, Farkaad A. Kadir, Mohammed A. AlSaadi, Vincent K. S. Hsiao.

Investigation: Lina A. Al-Ani.

Methodology: Lina A. Al-Ani, Wageeh A. Yehye, Farkaad A. Kadir.

Resources: Wageeh A. Yehye, Farkaad A. Kadir, Najihah M. Hashim, Mohammed A. AlSaadi, Nurhidayatullaili M. Julkapli, Vincent K. S. Hsiao.

Writing – original draft: Lina A. Al-Ani, Wageeh A. Yehye.

Writing – review & editing: Lina A. Al-Ani, Wageeh A. Yehye, Farkaad A. Kadir, Najihah M. Hashim, Mohammed A. AlSaadi, Nurhidayatullaili M. Julkapli, Vincent K. S. Hsiao.

References

1. Feng L, Liu Z. Graphene in biomedicine: opportunities and challenges. Nanomedicine. 2011; 6 (2):317–24. https://doi.org/10.2217/nnm.10.158 PMID: 21385134
2. Zhu Y, Murali S, Cai W, Li X, Suk JW, Potts JR, et al. Graphene and graphene oxide: synthesis, properties, and applications. Advanced materials. 2010; 22(35):3906–24. https://doi.org/10.1002/adma.201001068 PMID: 20706983
3. Weiss NO, Zhou H, Liao L, Liu Y, Jiang S, Huang Y, et al. Graphene: an emerging electronic material. Advanced materials. 2012; 24(43):5782–825. https://doi.org/10.1002/adma.201201482 PMID: 22930422
4. Chang H, Wu H. Graphene-Based Nanomaterials: Synthesis, Properties, and Optical and Optoelectronic Applications. Advanced Functional Materials. 2013; 23(16):1984–97.
5. Shinohara H, Tiwari A, Sharon M, Sharon M. Graphene: An Introduction to the Fundamentals and Industrial Applications: John Wiley & Sons; 2015.
6. Siegel RL, Miller KD, Jemal A. Cancer statistics, 2017. CA: a cancer journal for clinicians. 2017; 67 (1):7–30.
7. Stewart B, Wild CP. World cancer report 2014. Self. 2018.
8. Liu Z, Robinson JT, Sun X, Dai H. PEGylated nanographene oxide for delivery of water-insoluble cancer drugs. Journal of the American Chemical Society. 2008; 130(33):10876–7. https://doi.org/10.1021/ja803688x PMID: 18661992
9. Zhao X, Yang L, Li X, Jia X, Liu L, Zeng J, et al. Functionalized graphene oxide nanoparticles for cancer cell-specific delivery of antitumor drug. Bioconjugate chemistry. 2015; 26(1):128–36. https://doi.org/10.1021/bc5005137 PMID: 25525819
10. Orecchioni M, Cabizza R, Bianco A, Delogu LG. Graphene as cancer theranostic tool: progress and future challenges. Theranostics. 2015; 5(7):710. https://doi.org/10.7150/thno.11387 PMID: 25897336
11. Wang C, Li J, Amatore C, Chen Y, Jiang H, Wang XM. Gold nanoclusters and graphene nanocomposites for drug delivery and imaging of cancer cells. Angewandte Chemie International Edition. 2011; 50 (49):11644–8. https://doi.org/10.1002/anie.201105573 PMID: 21990208
12. Novoselov KS, Fal V, Colombo L, Gellert P, Schwab M, Kim K. A roadmap for graphene. nature. 2012; 490(7419):192. https://doi.org/10.1038/nature11458 PMID: 23060189
13. George G, Sisupal SB, Tomy T, Kumaran A, Vadivelu P, Suvekbala V, et al. Facile, environmentally benign and scalable approach to produce pristine few layers graphene suitable for preparing biocompatible polymer nanocomposites. Scientific reports. 2018; 8(1):11228. https://doi.org/10.1038/s41598-018-28560-1 PMID: 30046158
14. Tien H-W, Huang Y-L, Yang S-Y, Wang J-Y, Ma C-CM. The production of graphene nanosheets decorated with silver nanoparticles for use in transparent, conductive films. Carbon. 2011; 49(5):1550–60.
15. Saikia I, Sonowal S, Pal M, Boruah PK, Das MR, Tamuly C. Biosynthesis of gold decorated reduced graphene oxide and its biological activities. Materials Letters. 2016; 178:239–42.
16. Some S, Gwon A-R, Hwang E, Bahn G-h, Yoon Y, Kim Y, et al. Cancer therapy using ultrahigh hydrophobic drug-loaded graphene derivatives. Scientific reports. 2014; 4:6314. https://doi.org/10.1038/srep06314 PMID: 25204358

17. Choi Y-J, Gurunathan S, Kim J-H. Graphene oxide–silver nanocomposite enhances cytotoxic and apoptotic potential of salinomycin in human ovarian cancer stem cells (OvCSCs): A novel approach for cancer therapy. International journal of molecular sciences. 2018; 19(3):710.
18. Woolley AT. Biomedical microdevices and nanotechnology. Trends in Biotechnology. 2001; 19(2):38–9. PMID: 11252264
19. Boisseau P, Loubaton B. Nanomedicine, nanotechnology in medicine. Comptes Rendus Physique. 2011; 12(7):620–36.
20. McCallion C, Burthem J, Rees-Unwin K, Golovanov A, Pluen A. Graphene in therapeutics delivery: problems, solutions and future opportunities. European Journal of Pharmaceutics and Biopharmaceutics. 2016; 104:235–50. https://doi.org/10.1016/j.ejpb.2016.04.015 PMID: 27113141
21. Depan D, Shah J, Misra R. Controlled release of drug from folate-decorated and graphene mediated drug delivery system: synthesis, loading efficiency, and drug release response. Materials Science and Engineering: C. 2011; 31(7):1305–12.
22. Wahab R, Dwivedi S, Khan F, Mishra YK, Hwang I, Shin H-S, et al. Statistical analysis of gold nanoparticle-induced oxidative stress and apoptosis in myoblast (C2C12) cells. Colloids and surfaces B: Biointerfaces. 2014; 123:664–72. https://doi.org/10.1016/j.colsurfb.2014.10.012 PMID: 25456994
23. Patra CR, Bhattacharya R, Mukhopadhyay D, Mukherjee P. Fabrication of gold nanoparticles for targeted therapy in pancreatic cancer. Advanced drug delivery reviews. 2010; 62(3):346–61. https://doi.org/10.1016/j.addr.2009.11.007 PMID: 19914317
24. AshaRani P, Low Kah Mun G, Hande MP, Valiyaveettil S. Cytotoxicity and genotoxicity of silver nanoparticles in human cells. ACS nano. 2008; 3(2):279–90.
25. Song J, Yang X, Jacobson O, Lin L, Huang P, Niu G, et al. Sequential drug release and enhanced photothermal and photoacoustic effect of hybrid reduced graphene oxide-loaded ultrasmall gold nanorod vesicles for cancer therapy. 2015. https://doi.org/10.1021/acsnano.5b03804 PMID: 26308265
26. Wang X, Han Q, Yu N, Li J, Yang L, Yang R, et al. Aptamer–conjugated graphene oxide–gold nanocomposites for targeted chemo-photothermal therapy of cancer cells. Journal of Materials Chemistry B. 2015; 3(19):4036–42.
27. Xu C, Yang D, Mei L, Li Q, Zhu H, Wang T. Targeting chemophotothermal therapy of hepatoma by gold nanorods/graphene oxide core/shell nanocomposites. ACS applied materials & interfaces. 2013; 5(24):12911–20.
28. Yuan Y, Zhang Y, Liu B, Wu H, Kang Y, Li M, et al. The effects of multifunctional MiR-122-loaded graphene-gold composites on drug-resistant liver cancer. Journal of nanobiotechnology. 2015; 13(1):12.
29. Ma X, Qu Q, Zhao Y, Luo Z, Zhao Y, Ng KW, et al. Graphene oxide wrapped gold nanoparticles for intracellular Raman imaging and drug delivery. Journal of Materials Chemistry B. 2013; 1(47):6495–500.
30. Zhu X, Xu X, Liu F, Jin J, Liu L, Zhi Y, et al. Green synthesis of graphene nanosheets and their in vitro cytotoxicity against human prostate cancer (DU 145) cell lines. Nanomaterials and Nanotechnology. 2017; 7:1847980417702794.
31. Bhattacherjee A, Ghosh T, Datta A. Green synthesis and characterisation of antioxidant-tagged gold nanoparticle (X-GNP) and studies on its potent antimicrobial activity. Journal of Experimental Nanoscience. 2018; 13(1):50–61.
32. Prasad S, Aggarwal BB. Turmeric, the golden spice. 2011. PMID: 22593922
33. Unlu A, Nayir E, Kalenderoglu MD, Kirca O, Ozdogan M. Curcumin (Turmeric) and cancer. Journal of buon–2016–21 (5)–P. 2016:1050–60.
34. Kunnumakkara AB, Anand P, Aggarwal BB. Curcumin inhibits proliferation, invasion, angiogenesis and metastasis of different cancers through interaction with multiple cell signaling proteins. Cancer letters. 2008; 269(2):199–225. https://doi.org/10.1016/j.canlet.2008.03.009 PMID: 18479807
35. Heger M, van Golen RF, Broekgaarden M, Michel MC. The molecular basis for the pharmacokinetics and pharmacodynamics of curcumin and its metabolites in relation to cancer. Pharmacological reviews. 2014; 66(1):222–307. https://doi.org/10.1124/pr.110.004044 PMID: 24368738
36. Yallapu MM, Jaggi M, Chauhan SC. Curcumin nanoformulations: a future nanomedicine for cancer. Drug discovery today. 2012; 17(1):71–80.
37. Ramazani A, Abrvash M, Sadighian S, Rostamizadeh K, Fathi M. Preparation and characterization of curcumin loaded gold/graphene oxide nanocomposite for potential breast cancer therapy. Research on Chemical Intermediates. 2018; 44(12):7891–904.
38. Malekmohammadi S, Hadadzadeh H, Farrokhpour H, Amirghofran Z. Immobilization of gold nanoparticles on folate-conjugated dendritic mesoporous silica-coated reduced graphene oxide nanosheets: a

new nanoplatform for curcumin pH-controlled and targeted delivery. Soft matter. 2018; 14(12):2400–10. https://doi.org/10.1039/c7sm02248d PMID: 29512668

39. Patlolla A, Rondalph J, Tchounwou P. Biochemical and Histopathological Evaluation of Graphene Oxide in Sprague-Dawley Rats. Austin journal of environmental toxicology. 2017; 3(1). PMID: 29503980

40. Rao CNR, Sood AK. Graphene: synthesis, properties, and phenomena: John Wiley & Sons; 2013.

41. Cos P, Vlietinck AJ, Berghe DV, Maes L. Anti-infective potential of natural products: how to develop a stronger in vitro 'proof-of-concept'. Journal of ethnopharmacology. 2006; 106(3):290–302. https://doi.org/10.1016/j.jep.2006.04.003 PMID: 16698208

42. Marcano DC, Kosynkin DV, Berlin JM, Sinitskii A, Sun Z, Slesarev A, et al. Improved synthesis of graphene oxide. ACS nano. 2010; 4(8):4806–14. https://doi.org/10.1021/nn1006368 PMID: 20731455

43. Chuang M-K, Lin S-W, Chen F-C, Chu C-W, Hsu C-S. Gold nanoparticle-decorated graphene oxides for plasmonic-enhanced polymer photovoltaic devices. Nanoscale. 2014; 6(3):1573–9. https://doi.org/10.1039/c3nr05077g PMID: 24326523

44. Grabar KC, Freeman RG, Hommer MB, Natan MJ. Preparation and characterization of Au colloid monolayers. Analytical chemistry. 1995; 67(4):735–43.

45. Magalhães LM, Santos F, Segundo MA, Reis S, Lima JL. Rapid microplate high-throughput methodology for assessment of Folin-Ciocalteu reducing capacity. Talanta. 2010; 83(2):441–7. https://doi.org/10.1016/j.talanta.2010.09.042 PMID: 21111158

46. Sanna V, Pala N, Dessì G, Manconi P, Mariani A, Dedola S, et al. Single-step green synthesis and characterization of gold-conjugated polyphenol nanoparticles with antioxidant and biological activities. International journal of nanomedicine. 2014; 9:4935. https://doi.org/10.2147/IJN.S70648 PMID: 25364251

47. Sharma OP, Bhat TK. DPPH antioxidant assay revisited. Food chemistry. 2009; 113(4):1202–5.

48. Saikia JP, Paul S, Konwar BK, Samdarshi SK. Ultrasonication: Enhances the antioxidant activity of metal oxide nanoparticles. Colloids and Surfaces B: Biointerfaces. 2010; 79(2):521–3. https://doi.org/10.1016/j.colsurfb.2010.04.022 PMID: 20537871

49. Liao K-H, Lin Y-S, Macosko CW, Haynes CL. Cytotoxicity of graphene oxide and graphene in human erythrocytes and skin fibroblasts. ACS applied materials & interfaces. 2011; 3(7):2607–15.

50. Badisa RB, Darling-Reed SF, Joseph P, Cooperwood JS, Latinwo LM, Goodman CB. Selective cytotoxic activities of two novel synthetic drugs on human breast carcinoma MCF-7 cells. Anticancer research. 2009; 29(8):2993–6. PMID: 19661306

51. Musa MA, Badisa VL, Latinwo LM, Waryoba C, Ugochukwu N. In vitro cytotoxicity of benzopyranone derivatives with basic side chain against human lung cell lines. Anticancer research. 2010; 30 (11):4613–7. PMID: 21115914

52. Goenka S, Sant V, Sant S. Graphene-based nanomaterials for drug delivery and tissue engineering. Journal of Controlled Release. 2014; 173:75–88. https://doi.org/10.1016/j.jconrel.2013.10.017 PMID: 24161530

53. Aggarwal BB, Surh Y-J, Shishodia S. The molecular targets and therapeutic uses of curcumin in health and disease: Springer Science & Business Media; 2007.

54. Guo W, Wu L, Fan K, Nie D, He W, Yang J, et al. Reduced Graphene Oxide-Gold Nanoparticle Nanoframework as a Highly Selective Separation Material for Aflatoxins. Scientific Reports. 2017; 7 (1):14484. https://doi.org/10.1038/s41598-017-15210-1 PMID: 29101380

55. Giasuddin A, Jhuma K, Haq AM. Use of gold nanoparticles in diagnostics, surgery and medicine: a review. Bangladesh J Med Biochem. 2012; 5(2):56–60.

56. Verma SK, Jha E, Panda PK, Kumari P, Pramanik N, Kumari S, et al. Molecular investigation to RNA and protein based interaction induced in vivo biocompatibility of phytofabricated AuNP with embryonic zebrafish. Artificial cells, nanomedicine, and biotechnology. 2018; 46(sup3):S671–S84. https://doi.org/10.1080/21691401.2018.1505746 PMID: 30311784

57. Torres-Mendieta R, Ventura-Espinosa D, Sabater S, Lancis J, Mínguez-Vega G, Mata JA. In situ decoration of graphene sheets with gold nanoparticles synthetized by pulsed laser ablation in liquids. Scientific reports. 2016; 6:30478. https://doi.org/10.1038/srep30478 PMID: 27464997

58. Verma SK, Jha E, Sahoo B, Panda PK, Thirumurugan A, Parashar S, et al. Mechanistic insight into the rapid one-step facile biofabrication of antibacterial silver nanoparticles from bacterial release and their biogenicity and concentration-dependent in vitro cytotoxicity to colon cells. RSC Advances. 2017; 7(64):40034–45.

59. Verma SK, Jha E, Panda PK, Thirumurugan A, Patro S, Parashar S, et al. Molecular insights to alkaline based bio-fabrication of silver nanoparticles for inverse cytotoxicity and enhanced antibacterial activity. Materials Science and Engineering: C. 2018; 92:807–18.

60. Kumari P, Panda PK, Jha E, Pramanik N, Nisha K, Kumari K, et al. Molecular insight to in vitro biocompatibility of phytofabricated copper oxide nanoparticles with human embryonic kidney cells. Nanomedicine. 2018; 13(19):2415–33. https://doi.org/10.2217/nnm-2018-0175 PMID: 30251920

61. Shaabani E, Amini SM, Kharrazi S, Tajerian R. Curcumin coated gold nanoparticles: synthesis, characterization, cytotoxicity, antioxidant activity and its comparison with citrate coated gold nanoparticles. Nanomedicine Journal. 2017; 4(2):115–25.

62. Goncalves G, Marques PA, Granadeiro CM, Nogueira HI, Singh M, Gracio J. Surface modification of graphene nanosheets with gold nanoparticles: the role of oxygen moieties at graphene surface on gold nucleation and growth. Chemistry of Materials. 2009; 21(20):4796–802.

63. Sindhu K, Rajaram A, Sreeram K, Rajaram R. Curcumin conjugated gold nanoparticle synthesis and its biocompatibility. RSC Advances. 2014; 4(4):1808–18.

64. Hatamie S, Akhavan O, Sadrnezhaad SK, Ahadian MM, Shirolkar MM, Wang HQ. Curcumin-reduced graphene oxide sheets and their effects on human breast cancer cells. Materials Science and Engineering: C. 2015; 55:482–9.

65. Hayyan M, Abo-Hamad A, AlSaadi MA, Hashim MA. Functionalization of graphene using deep eutectic solvents. Nanoscale research letters. 2015; 10(1):324.

66. Dresselhaus MS, Jorio A, Hofmann M, Dresselhaus G, Saito R. Perspectives on carbon nanotubes and graphene Raman spectroscopy. Nano letters. 2010; 10(3):751–8. https://doi.org/10.1021/nl904286r PMID: 20085345

67. Ferrari AC. Raman spectroscopy of graphene and graphite: disorder, electron–phonon coupling, doping and nonadiabatic effects. Solid state communications. 2007; 143(1):47–57.

68. Armas LE, Zamarion VM, Quispe LT, Otero EP, Menezes J, Zegarra LB, et al. Effect of Gold Nanoparticles and Unwanted Residues on Raman Spectra of Graphene Sheets. Brazilian Journal of Physics. 2018; 48(5):477–84.

69. Lee J, Novoselov KS, Shin HS. Interaction between metal and graphene: dependence on the layer number of graphene. ACS nano. 2010; 5(1):608–12. https://doi.org/10.1021/nn103004c PMID: 21174405

70. Kalbac M, Vales V, Vejpravova J. The effect of a thin gold layer on graphene: a Raman spectroscopy study. RSC Advances. 2014; 4(105):60929–35.

71. Konios D, Stylianakis MM, Stratakis E, Kymakis E. Dispersion behaviour of graphene oxide and reduced graphene oxide. Journal of colloid and interface science. 2014; 430:108–12. https://doi.org/10.1016/j.jcis.2014.05.033 PMID: 24998061

72. Sharma N, Sharma V, Jain Y, Kumari M, Gupta R, Sharma S, et al., editors. Synthesis and characterization of graphene oxide (GO) and reduced graphene oxide (rGO) for gas sensing application. Macromolecular Symposia; 2017: Wiley Online Library.

73. Zhang H, Hines D, Akins DL. Synthesis of a nanocomposite composed of reduced graphene oxide and gold nanoparticles. Dalton Transactions. 2014; 43(6):2670–5. https://doi.org/10.1039/c3dt52573b PMID: 24336741

74. Bai RG, Muthoosamy K, Zhou M, Ashokkumar M, Huang NM, Manickam S. Sonochemical and sustainable synthesis of graphene-gold (G-Au) nanocomposites for enzymeless and selective electrochemical detection of nitric oxide. Biosensors and Bioelectronics. 2017; 87:622–9. https://doi.org/10.1016/j.bios.2016.09.003 PMID: 27616288

75. Dorniani D, Saifullah B, Barahuie F, Arulselvan P, Hussein MZB, Fakurazi S, et al. Graphene oxide-gallic acid nanodelivery system for cancer therapy. Nanoscale research letters. 2016; 11(1):491. https://doi.org/10.1186/s11671-016-1712-2 PMID: 27822913

76. Siddhardha RS, Kumar VL, Kaniyoor A, Muthukumar VS, Ramaprabhu S, Podila R, et al. Synthesis and characterization of gold graphene composite with dyes as model substrates for decolorization: A surfactant free laser ablation approach. Spectrochimica Acta Part A: Molecular and Biomolecular Spectroscopy. 2014; 133:365–71.

77. Movahed SK, Fakharian M, Dabiri M, Bazgir A. Gold Nanoparticles Decorated Reduced Graphene Oxide Sheets with Significantly High Catalytic Activity for Ullmann Homocoupling.

78. Ding J, Liu Y, Yuan N, Ding G, Fan Y, Yu C. The influence of temperature, time and concentration on the dispersion of reduced graphene oxide prepared by hydrothermal reduction. Diamond and Related Materials. 2012; 21:11–5.

79. Verma HN, Singh P, Chavan R. Gold nanoparticle: synthesis and characterization. Veterinary world. 2014; 7(2):72–7.

80. Naebe M, Wang J, Amini A, Khayyam H, Hameed N, Li LH, et al. Mechanical property and structure of covalent functionalised graphene/epoxy nanocomposites. Scientific reports. 2014; 4:4375. https://doi.org/10.1038/srep04375 PMID: 24625497

81. Loryuenyong V, Totepvimarn K, Eimburanapravat P, Boonchompoo W, Buasri A. Preparation and characterization of reduced graphene oxide sheets via water-based exfoliation and reduction methods. Advances in Materials Science and Engineering. 2013;2013.

82. Zhang C, Chen M, Xu X, Zhang L, Zhang L, Xia F, et al. Graphene oxide reduced and modified by environmentally friendly glycylglycine and its excellent catalytic performance. Nanotechnology. 2014; 25(13):135707. https://doi.org/10.1088/0957-4484/25/13/135707 PMID: 24598357

83. GIRI A, GOSWAMI N, SARKAR S, PAL SK. Bio–Nanomaterials: Understanding Key Biophysics and Their Applications. Nanotechnology. 11:41–110.

84. Amaro-Gahete J, Benítez A, Otero R, Esquivel D, Jiménez-Sanchidrián C, Morales J, et al. A Comparative Study of Particle Size Distribution of Graphene Nanosheets Synthesized by an Ultrasound-Assisted Method. Nanomaterials. 2019; 9(2):152.

85. Gurunathan S, Han JW, Dayem AA, Eppakayala V, Kim J-H. Oxidative stress-mediated antibacterial activity of graphene oxide and reduced graphene oxide in Pseudomonas aeruginosa. International journal of nanomedicine. 2012; 7:5901. https://doi.org/10.2147/IJN.S37397 PMID: 23226696

86. Lammel T, Boisseaux P, Fernández-Cruz M-L, Navas JM. Internalization and cytotoxicity of graphene oxide and carboxyl graphene nanoplatelets in the human hepatocellular carcinoma cell line Hep G2. Particle and fibre toxicology. 2013; 10(1):27.

87. Kashyap S, Mishra S, Behera SK. Aqueous colloidal stability of graphene oxide and chemically converted graphene. Journal of Nanoparticles. 2014;2014.

88. Tokusoglu O, Simsek A, Parvizi M, Eymen D. Turmeric curcuminoid polyphenolics as antioxidant and anticarcinogenic agents. Natural Science and Discovery. 2015; 1(3):56–61.

89. Borra SK, Gurumurthy P, Mahendra J. Antioxidant and free radical scavenging activity of curcumin determined by using different in vitro and ex vivo models. Journal of Medicinal Plants Research. 2013; 7(36):2680–90.

90. Pathak L, Kanwal A, Agrawal Y. Curcumin loaded self assembled lipid-biopolymer nanoparticles for functional food applications. Journal of food science and technology. 2015; 52(10):6143–56. https://doi.org/10.1007/s13197-015-1742-2 PMID: 26396362

91. Ak T, Gülçin İ. Antioxidant and radical scavenging properties of curcumin. Chemico-biological interactions. 2008; 174(1):27–37. https://doi.org/10.1016/j.cbi.2008.05.003 PMID: 18547552

92. Mathew A, Fukuda T, Nagaoka Y, Hasumura T, Morimoto H, Yoshida Y, et al. Curcumin loaded-PLGA nanoparticles conjugated with Tet-1 peptide for potential use in Alzheimer's disease. PLoS one. 2012; 7(3):e32616. https://doi.org/10.1371/journal.pone.0032616 PMID: 22403681

93. López-Lázaro M. Anticancer and carcinogenic properties of curcumin: considerations for its clinical development as a cancer chemopreventive and chemotherapeutic agent. Molecular nutrition & food research. 2008; 52(S1):S103–S27.

94. Sundararajan B, Mahendran G, Thamaraiselvi R, Kumari BR. Biological activities of synthesized silver nanoparticles from Cardiospermum halicacabum L. Bulletin of Materials Science. 2016; 39(2):423–31.

95. Goodarzi V, Zamani H, Bajuli L, Moradshahi A. Evaluation of antioxidant potential and reduction capacity of some plant extracts in silver nanoparticles' synthesis. Molecular biology research communications. 2014; 3(3):165. PMID: 27843980

96. Nagaich U, Gulati N, Chauhan S. Antioxidant and antibacterial potential of silver nanoparticles: biogenic synthesis utilizing apple extract. Journal of pharmaceutics. 2016;2016.

97. Kumar A, Singh M, Singh P, Singh S, Raj P, Pandey K. Antioxidant efficacy and curcumin content of turmeric (Curcuma-longa L.) flower. International Journal of Current Pharmaceutical Research. 2016; 8(3):112–4.

98. Priya R, Balachandran S, Vineetha V, Raghu K, Vigneshwar M, Annaraj J, et al. The possible role of reactive centers of curcumin in deciding its biological activity. J Mater Sci Eng. 2014; 10:269–78.

99. Qiu Y, Wang Z, Owens AC, Kulaots I, Chen Y, Kane AB, et al. Antioxidant chemistry of graphene-based materials and its role in oxidation protection technology. Nanoscale. 2014; 6(20):11744–55. https://doi.org/10.1039/c4nr03275f PMID: 25157875

100. Kurt BZ, Durmus Z, Durmus A. Preparation and characterization of platinum (Pt) and palladium (Pd) nanoparticle decorated graphene sheets and their utilization for the elimination of basic fuchsin and indigo carmine dyes. Solid State Sciences. 2016; 51:51–8.

101. Suresh D, Nethravathi P, Nagabhushana H, Sharma S. Spinach assisted green reduction of graphene oxide and its antioxidant and dye absorption properties. Ceramics International. 2015; 41(3):4810–3.

102. Nie Z, Liu KJ, Zhong C-J, Wang L-F, Yang Y, Tian Q, et al. Enhanced radical scavenging activity by antioxidant-functionalized gold nanoparticles: a novel inspiration for development of new artificial antioxidants. Free Radical Biology and Medicine. 2007; 43(9):1243–54. https://doi.org/10.1016/j.freeradbiomed.2007.06.011 PMID: 17893037

103. Wang D, Markus J, Kim Y-J, Wang C, Pérez ZEJ, Ahn S, et al. coalescence of functional gold and monodisperse silver nanoparticles mediated by black Panax ginseng Meyer root extract. International Journal of Nanomedicine. 2016; 11:6621. https://doi.org/10.2147/IJN.S113692 PMID: 28008248

104. Razzaq H, Saira F, Yaqub A, Qureshi R, Mumtaz M, Saleemi S. Interaction of gold nanoparticles with free radicals and their role in enhancing the scavenging activity of ascorbic acid. Journal of Photochemistry and Photobiology B: Biology. 2016; 161:266–72.

105. Siddiqi NJ, Abdelhalim MAK, AlYafee YA, Alhomida AS. Studies on the effect of gold nanoparticles on oxidative stress and antioxidants defense indices in various rat tissues. African Journal of Pharmacy and Pharmacology. 2012; 6(47):3246–51.

106. Fukuta M, Kanamori S, Furukawa T, Nawa Y, Inami W, Lin S, et al. Dynamic nano-imaging of label-free living cells using electron beam excitation-assisted optical microscope. Scientific reports. 2015; 5:16068. https://doi.org/10.1038/srep16068 PMID: 26525841

107. Alberts B, Bray D, Hopkin K, Johnson AD, Lewis J, Raff M, et al. Essential cell biology: Garland Science; 2013.

108. Jaworski S, Sawosz E, Grodzik M, Winnicka A, Prasek M, Wierzbicki M, et al. In vitro evaluation of the effects of graphene platelets on glioblastoma multiforme cells. International journal of nanomedicine. 2013; 8:413. https://doi.org/10.2147/IJN.S39456 PMID: 23378763

109. Drasler B, Sayre P, Steinhaeuser KG, Petri-Fink A, Rothen-Rutishauser B. In vitro approaches to assess the hazard of nanomaterials. NanoImpact. 2017; 8:99–116.

110. Riebeling C, Piret J-P, Trouiller B, Nelissen I, Saout C, Toussaint O, et al. A guide to nanosafety testing: Considerations on cytotoxicity testing in different cell models. NanoImpact. 2018; 10:1–10.

111. Tominaga H, Ishiyama M, Ohseto F, Sasamoto K, Hamamoto T, Suzuki K, et al. A water-soluble tetrazolium salt useful for colorimetric cell viability assay. Analytical Communications. 1999; 36(2):47–50.

112. Tian C, Asghar S, Wu Y, Chen Z, Jin X, Yin L, et al. Improving intestinal absorption and oral bioavailability of curcumin via taurocholic acid-modified nanostructured lipid carriers. International journal of nanomedicine. 2017; 12:7897. https://doi.org/10.2147/IJN.S145988 PMID: 29138557

113. Kurita T, Makino Y. Novel curcumin oral delivery systems. Anticancer research. 2013; 33(7):2807–21. PMID: 23780965

114. Lee W-H, Loo C-Y, Young PM, Traini D, Mason RS, Rohanizadeh R. Recent advances in curcumin nanoformulation for cancer therapy. Expert opinion on drug delivery. 2014; 11(8):1183–201. https://doi.org/10.1517/17425247.2014.916686 PMID: 24857605

115. Guo X, Mei N. Assessment of the toxic potential of graphene family nanomaterials. Journal of food and drug analysis. 2014; 22(1):105–15. https://doi.org/10.1016/j.jfda.2014.01.009 PMID: 24673908

116. Lin K-C, Lin M-W, Hsu M-N, Yu-Chen G, Chao Y-C, Tuan H-Y, et al. Graphene oxide sensitizes cancer cells to chemotherapeutics by inducing early autophagy events, promoting nuclear trafficking and necrosis. Theranostics. 2018; 8(9):2477. https://doi.org/10.7150/thno.24173 PMID: 29721093

117. Li R, Zhang L, Wang P. Rational design of nanomaterials for water treatment. Nanoscale. 2015; 7 (41):17167–94. https://doi.org/10.1039/c5nr04870b PMID: 26437738

118. Manocha L, Valand J, Patel N, Warrier A, Manocha S. Nanocomposites for structural applications. 2006.

119. Marson RL, Nguyen TD, Glotzer SC. Rational design of nanomaterials from assembly and reconfigurability of polymer-tethered nanoparticles. MRS Communications. 2015; 5(3):397–406.

120. Sadanandam A, Lyssiotis CA, Homicsko K, Collisson EA, Gibb WJ, Wullschleger S, et al. A colorectal cancer classification system that associates cellular phenotype and responses to therapy. Nature medicine. 2013; 19(5):619. https://doi.org/10.1038/nm.3175 PMID: 23584089

121. De S, Mohanty S, Nayak SK, Verma SK, Suar M. Nanotoxicity of Rare Earth Metal Oxide Anchored Graphene Nanohybrid: A Facile Synthesis and In Vitro Cellular Response Studies. Nano. 2015; 10 (06):1550091.

122. Singh M, Gupta P, Baronia R, Singh P, Karuppiah S, Shankar R, et al. In vitro cytotoxicity of GO–DOx on FaDu squamous carcinoma cell lines. International journal of nanomedicine. 2018; 13(T-NANO 2014 Abstracts):107. https://doi.org/10.2147/IJN.S124891 PMID: 29593407

123. Zhang B, Wei P, Zhou Z, Wei T. Interactions of graphene with mammalian cells: Molecular mechanisms and biomedical insights. Advanced drug delivery reviews. 2016; 105:145–62. https://doi.org/10.1016/j.addr.2016.08.009 PMID: 27569910

124. Shim G, Kim M-G, Park JY, Oh Y-K. Graphene-based nanosheets for delivery of chemotherapeutics and biological drugs. Advanced drug delivery reviews. 2016; 105:205–27. https://doi.org/10.1016/j.addr.2016.04.004 PMID: 27085467

125. Sreevalsan S, Safe S. Reactive oxygen species and colorectal cancer. Current colorectal cancer reports. 2013; 9(4):350–7. https://doi.org/10.1007/s11888-013-0190-5 PMID: 25584043

126. Ghalandarlaki N, Alizadeh AM, Ashkani-Esfahani S. Nanotechnology-applied curcumin for different diseases therapy. BioMed Research International. 2014;2014.

127. Yallapu MM, Nagesh PKB, Jaggi M, Chauhan SC. Therapeutic applications of curcumin nanoformulations. The AAPS journal. 2015; 17(6):1341–56. https://doi.org/10.1208/s12248-015-9811-z PMID: 26335307

128. Dai C, Li D, Gong L, Xiao X, Tang S. Curcumin ameliorates furazolidone-induced DNA damage and apoptosis in human hepatocyte L02 cells by inhibiting ROS production and mitochondrial pathway. Molecules. 2016; 21(8):1061.

129. Verma SK, Jha E, Panda PK, Thirumurugan A, Parashar S, Patro S, et al. Mechanistic insight into size-dependent enhanced cytotoxicity of industrial antibacterial titanium oxide nanoparticles on colon cells because of reactive oxygen species quenching and neutral lipid alteration. ACS omega. 2018; 3 (1):1244–62. https://doi.org/10.1021/acsomega.7b01522 PMID: 30023799

130. Verma SK, Panda PK, Jha E, Suar M, Parashar S. Altered physiochemical properties in industrially synthesized ZnO nanoparticles regulate oxidative stress; induce in vivo cytotoxicity in embryonic zebrafish by apoptosis. Scientific reports. 2017; 7(1):13909. https://doi.org/10.1038/s41598-017-14039-y PMID: 29066782

131. Verma SK, Jha E, Panda PK, Mukherjee M, Thirumurugan A, Makkar H, et al. Mechanistic insight into ROS and neutral lipid alteration induced toxicity in the human model with fins (Danio rerio) by industrially synthesized titanium dioxide nanoparticles. Toxicology research. 2018; 7(2):244–57. https://doi.org/10.1039/c7tx00300e PMID: 30090579